RSC Advances

PAPER

View Article Online
View Journal | View Issue

Cite this: *RSC Adv.*, 2020, **10**, 2283

Molecular probe dynamics and free volume heterogeneities in n-propanol confined in a regular MCM-41 matrix by ESR and PALS

Josef Bartoš, *[a] Helena Švajdlenková[a] and Ondrej Šauša [b]

Received 14th November 2019
Accepted 17th December 2019

DOI: 10.1039/c9ra09495d

rsc.li/rsc-advances

A combined investigation of the spin probe TEMPO mobility and the free volume holes in *n*-propanol (*n*-PrOH) confined in a regular virgin MCM-41 matrix by means of ESR or PALS techniques, respectively, is reported. Dynamics of spin probe TEMPO alters at several characteristic ESR temperatures which are close to the characteristic PALS ones reflecting the changes in *o*-Ps annihilation and the related free volume. Correlations between these characteristic ESR and PALS temperatures indicate the common physical origins of the respective changes in the free volume expansion and the TEMPO mobility in the confined liquid *n*-PrOH. The significant difference in dynamic heterogeneity of TEMPO after confinement and free volume dispersion reflect the strongly altered structural-dynamic relationships in the confined *n*-PrOH medium with respect to the bulk situation.

1. Introduction

The topic of bulk *vs.* confined organic materials is currently studied by a variety of classic experimental techniques.[1–6] Changes in thermodynamic[1–4] and dynamic properties[5,6] which concern the phase and dynamics transitions and eventually, a formation of new phase(s) induced in confined organic medium (filler) by spatial limitation or/and by wall surface of confining inorganic matrix (confiner) are often found. On the basis of certain DSC, NMR as well as NS studies on some specific organic–inorganic hybrid systems it is considered that the important role is played by several distinct regions of the medium's entities in the confining matrix, such as contact pore surface layer (the layer adjacent to the pore wall) *i.e.*, interface and bulk-like central "core" region and sometimes intermediate one of the pore, the so-called interphase region.[3,4,6] At present, it is generally accepted that the overall confinement effect on organic media appears to be a result of the complex mutual interplay of the following two main factors: (i) geometric restriction of the pores on the medium in a given matrix and (ii) the mutual two-component interaction of the medium's constituents with the pore surface wall of the matrix.[1–6]

The bulk *vs.* confinement problem can also be solved by non-standard techniques utilizing some of special extrinsic microscopic probes inserted into the confined medium.[7–9] Among the smallest ones belong quasi-atomic sized *ortho*-positronium (*o*-Ps)[10] and stable molecular free radicals, the so-called spin probes of nitroxide type,[11] while the rather large ones are representented by fluorescence probes.[12] The first probe provides the information about the free volume microstructure and its changes with varying internal and external parameters within various organic media in their bulk state[10] as well as in various confined ones through its annihilation behavior[13–17] using positron annihilation lifetime spectroscopy (PALS). PALS response, *i.e.*, *o*-Ps lifetime, τ_3, as a function of temperature, exhibits several regions of different thermal behavior defining the characteristic PALS temperatures within solid (ordered crystal or disordered glass) and disordered liquid state, such as T_{bi}^{G}, T_{g}^{PALS} and T_{bi}^{L}.[18] These characteristic PALS temperatures mark the changes in free volume expansion within the glassy and liquids state of the amorphous phase as well as at the glass to liquid transition. In the latter technique, the dynamics as well as the interaction of some nitroxide spin probes in several simple organic fillers embeded in various confiners can effectively be investigated by electron spin resonance spectroscopy (ESR).[19–23] Similarly as in PALS, several changes in the spectral features of a quasi-spherical spin probe, namely, 2,2,6,6-tetramethyl-piperidinyl-1-oxy (TEMPO) occur in the $2A_{zz'}$ *vs.* T plot at the characteristic ESR temperatures, where $A_{zz'}$ is the *z*-component of the hyperfine coupling (hfc) constant between the unpaired electron and the nitrogen nucleus in the >N–O˙ fragment, A. These are marked as $T_{Xi}^{slow,A_{zz}}$ and $T_{Xi}^{fast,A_{zz}}$ in the slow or fast motion regime, respectively, and they reflect the changes in its magnetic anisotropy due to molecular motion in a given organic medium within the respective motional regime as well as the conventionally defined characteristic ESR temperature $T_{50\ G}$ describing a transition between these motional regimes, *i.e.*, the temperature at which the z-component of the hyperfine coupling constant tensor, $2A_{zz'}$, reaches just the value of 50 Gauss corresponding to the time scale of reorientation of a few

[a]*Polymer Institute of SAS, Dúbravská Cesta 9, SK-845 41 Bratislava, Slovakia. E-mail: Jozef.Bartos@savba.sk*

[b]*Institute of Physics of SAS, Dúbravská Cesta 9, SK-845 11 Bratislava, Slovakia*

ns. Similar changes in the Arrhenius plot of another spectral-dynamic quantity, namely, correlation time in the respective motion regimes, τ_c^{slow}, τ_c^{fast} at the corresponding characteristic ESR temperatures, $T_{Xi}^{slow,\tau}$ and $T_{Xi}^{fast,\tau}$ were found.[24]

Recently, a synergic approach consisting in a combination of ESR and PALS techniques was used on a series of representatives of organic compounds of various structural types in the ordinary bulk state.[24–27] They included apolar or slightly polar compounds, *i.e.*, crystaline *n*-alkanes or amorphous polymers,[25] polar protic ones, *i.e.*, mono- and polyalcohols[24,26] and polar aprotic substances[27] of small molecular, oligomeric and polymer kinds. In some cases certain mutual relationships between the characteristic ESR and PALS temperatures, at which the spin probe dynamic and the microstructural free volume change in the bulk state, were found and their physical origin revealed.[28]

Finally, this synergic approach was very recently used also on apolar *n*-undecane (*n*-UND) in the bulk and confined states of two types of inorganic SiO_2-based matrices, namely, silica gels (SG) with virgin (polar hydrophilic) and modified (mostly apolar hydrophobic) pore surfaces.[29] This study revealed the importance of relative interaction between all the three components of the confined system. *i.e.*, not only between apolar or polar filler and apolar or polar confiner, but also between polar spin probe TEMPO and apolar or polar medium as well as apolar or polar matrix. Consequently, it is emphasized the suitable choice of the filler-confiner pair to get the reliable information about the altered structural-dynamic state of a given confined medium with respect to its reference bulk situation.

In previous studies, several apolar media, such as *n*-hexadecane (*n*-HXD),[22] *n*-UND[29] and cyclohexane (CHX)[30] and one polar medium, *n*-propanol (*n*-PrOH)[23] embeded in various silica gels with the irregular pore morphology, *i.e.*, a wide pore size distribution of the interconnected pores, were used. Thus, it is of actuality to verify the afore-mentioned combined ESR and PALS approach on further structural types of organic medium as well as on other pore morphologies of silica-based matrix.

This paper reports a joint ESR and PALS study of the molecular probe dynamics and the interaction as well as the annihilation behavior of the *o*-Ps in *n*-propanol (*n*-PrOH). This model substance was chosen as a representative of polar protic organic fillers confined in the regular SiO_2-based material, namely, MCM-41 matrix[31] with the narrow pore size distribution and the isolated (non-interconnected) cylinder-like channels as a representative of inorganic confiners. The aim is to reveal the characterization potential of confined organics as measured by polar spin probe using ESR technique by testing further combination of filler and confiner, namely, polar protic medium in a given polar matrix and how it is related to free volume microstructure of the same confined organic medium and its temperature development extracted from PALS.

2. Experimental

2.1 Materials

Anhydrous *n*-propanol (*n*-PrOH) from Sigma-Aldrich, Inc, Germany with the purity of 99.7% was used as a confined organic medium (filler). Regular virgin Mobil Composite Material, (MCM-41) matrix having the regular ordered cylinder-like channels with the mean pore size, $D_{pore} = 40$ Å from Sigma-Aldrich, Inc, Germany was utilized as a confining inorganic material.

The confined *n*-PrOH/MCM-41 system for PALS and the spin system for ESR studies was prepared step by step (drop by drop) filling of *n*-PrOH or of a dilute solution of the *n*-PrOH doped with the spin probe TEMPO, respectively, into the accessible pores of the MCM-41 matrix to achieve the fully filled (saturated) state. The capillary forces allowed to fill the accessible pores of matrices with *n*-PrOH under the situation with no liquid remained on the external surface of the silica grains. The theoretical and real mass fractions of the filler for the each filler/confiner system as well as the ratio of the latter quantity to the former one are given in Table 1. Before own filling procedure the MCM-41 matrix was dried at 393 K for several hours for the elimination of the majority of adsorbed moisture down to the saturation level as checked by middle-infrared spectroscopy.

2.2 Techniques

2.2.1 ESR. ESR measurements of the spin probed *n*-PrOH system were carried out on an X-band spectrometer Bruker ER 200 SRL operating at 9.4 GHz with a Bruker BVT 100 temperature controller unit. ESR spectra of the doped bulk *n*-PrOH/TEMPO solution and the doped confined *n*-PrOH/TEMPO/MCM-41 systems cooled from RT down to 100 K with approximately – 3 K min^{-1} were recorded in subsequent heating mode over a wide temperature range from 100 K up to 300 K with steps of 5–10 K. The measured sample was kept at the given temperature at thermal equilibrium before the ESR spectrum was accumulated. The temperature stability was ±0.5 K. The microwave power and the field modulation amplitude were optimized to avoid signal distortion. Analysis of the ESR spectra was performed in terms of the outermost (extrema) line separation of the triplet signal, $2A_{zz'}(T)$, as a function of temperature *via* WINEPR programme. Subsequently, the basic characteristic temperature ESR parameter $T_{50\ G}$[11,32] and some further ones $T_{Xi}^{slow,A_{zz}}$ and $T_{Xi}^{fast,A_{zz}}$[22–27] within both the slow or fast motion regimes, respectively, were determined. In addition, detailed simulations of the ESR spectra over a wide temperature range were carried out using the Non-Linear Shape Line (NLSL) program in order to determine the correlation times τ_{slow}, τ_{fast} and the relative population fractions F_{slow}, F_{fast}, of the spin probe TEMPO moving in the different, *i.e.*, slow, superposed and fast motion regions.[33] Analogously, the basic characteristic ESR temperature parameter T_c as well as further ones *i.e.*, $T_{Xi}^{slow,\tau}$, $T_{Xi}^{fast,\tau}$ describing all the three distinct motion regions, were evaluated.[24]

2.2.2 PALS. The PALS conventional fast–fast coincidence spectrometer was used for the measurements of *o*-Ps lifetime. The instrumental resolution function and source correction were made by defect-free Al sample. The resolution of the spectrometer is around 320 ps (FWHM).The standard sandwich arrangement of the sample chamber-positron source was used. Two identical sample chambers together with the positron source which was between them, were hermetically sealed and

Table 1 Physical parameters of MCM-41 matrix and *n*-PrOH/MCM-41 system

Matrix	Pore diameter D_{pore}, Å	Pore volume V_{pore}, $cm^3\ g^{-1}$	Pore area S_{pore}, $m^2\ g^{-1}$	$F_{n\text{-PrOH,theo}}$[a] (—)	$F_{n\text{-PrOH,sat}}$[b] (—)	X[c] %
MCM-41	40	0.80	1098	0.39	0.36	92.1

[a] $F_{n\text{-PrOH,theo}} = m_{n\text{-PrOH}}/(m_{n\text{-PrOH}} + m_{MCM\text{-}41})$, the theoretical mass fraction of *n*-PrOH medium with respect to the *n*-PrOH/MCM-41 system estimated using the density of *n*-PrOH at room temperature, $\rho_{n\text{-PrOH}}$ (RT) = 0.803 g cm^{-3} under the complete accessibility condition of all the pores for the *n*-PrOH medium. [b] $F_{n\text{-PrOH,sat}} = m_{n\text{-PrOH}}/(m_{n\text{-PrOH}} + m_{MCM\text{-}41})$, the real experimental mass fraction of *n*-PrOH in the *n*-PrOH/MCM-41 system corresponding to the fully filled (saturated) situation of the *n*-PrOH in the *n*-PrOH/MCM-41system. [c] $X = (F_{n\text{-PrOH,sat}}/F_{n\text{-PrOH,theo}}) \times 100\%$.

placed under vacuum in cryosystem between detectors of the spectrometer. In our case, the activity of the source ^{22}Na was 2 MBq. Despite the higher activity of the source, the frequency of coincidences is not so high due to rather large distance between detectors. Temperature measurements of the investigated samples were made in the helium closed-cycle refrigerator CCS-450 system from Janis. The temperature stability was about 0.2 K.

The bulk *n*-PrOH and the confined *n*-PrOH/MCM-41 samples were measured under the following two measuring cycles: (i) slow heating from T_{start} = 15 or 20 K up to room temperature (RT) after relative fast cooling with the average cooling rate $\Phi_c \sim -2.5$ K min^{-1} from RT and (ii) slow cooling from RT down to approximately T_{start} with a step of 5–10 K.

The Lifetime (LT) program, version LT polymers[34] was applied to evaluate the lifetime spectra into the three terms with the fixation of positronium relative intensities to 1 : 3, *i.e.*, relative contribution of *para*-positronium (*p*-Ps) to *ortho*-positronium (*o*-Ps) annihilation to the lifetime spectra. A short-time lifetime component from *p*-Ps was fixed to τ_1 = 0.125 ns, an intermediate-time one, τ_2, was attributed to the free positrons e^+ in bulk and free volume and defects, and finally, a long-time components, τ_3 and τ_4, originate from the *o*-Ps annihilation in free volumes of different sizes. The quasi-atomic sized *o*-Ps probe annihilates in organic materials by a pick-off process in which positron e^+ from the *o*-Ps annihilates with the electron e^- at the cavity surface, so that the *o*-Ps lifetime is shortened, depending on the shape of cavity and its characteristic size parameter(s).[35]

3. Results and discussion

3.1 Spectral behavior and reorientation dynamics of spin probe TEMPO in *n*-PrOH in the bulk and confined states in MCM-41 matrix

Fig. 1 displays the spectral evolution of the triplet signal of TEMPO in the saturated confined *n*-PrOH/MCM-41 system as a function temperature over a wide temperature range from 100 K up to 330 K. Similar result on the bulk *n*-PrOH was already reported in ref. 24. Typical change from a broad triplet stemming from the slow moving spin probes at relatively low temperatures to a narrow one from the fast reorienting ones in the high-*T* region is found.

The spectral behavior of both the studied spin systems, *i.e.*, the bulk *n*-PrOH + TEMPO system and the confined (*n*-PrOH + TEMPO)/MCM-41 one can be characterized by two quantities: (i) by *z*-component of the hyperfine coupling (hfc) constant, $2A_{zz'}$ and (ii) by correlation times τ_c^{slow}, τ_c^{fast} and relative fractions of the slow or/and fast moving spin probes, F_{slow}, F_{fast} as extracted from the NLSL simulations.

Fig. 2 displays the temperature dependence of $2A_{zz'}$ of the spin probe TEMPO in both *n*-PrOH in the bulk state and *n*-PrOH confined in the MCM-41 matrix as measured over a wide temperature range from 100 K up to 270 K or 330 K, respectively. The initially broad triplet in low-*T* region characterized by the high $2A_{zz'}$ values from the spin probes TEMPO moving in the slow motion regime changes towards the narrow triplet with the low values stemming from the spin probes TEMPO in the fast motion regime at relatively high-*T*s.[11] Although these $2A_{zz'}$ *vs.* *T* plots have in general the similar quasi-sigmoidal character, they exhibit some dramatic differences not only in the absolute $2A_{zz'}$ values at certain reference temperatures but also in the presence or the absence of various effects in its temperature dependence which define the characteristic ESR temperatures, $T_{Xi}^{slow,A_{zz}}$ and $T_{Xi}^{fast,A_{zz}}$. Thus, for the bulk *n*-PrOH, the $2A_{zz'}$ value at 100 K reaches 72.5 Gauss.[24] This is a typical value for the immobilized nitroxide probe in polar H-bonded media[11,26,28,36,37] which is significantly higher than that for apolar materials[11,25,35] due to the mutual polar and H-bonding interactions between the strongly polar molecules of TEMPO with the dipole moment μ_{TEMPO} = 3.0 debye[38] and the polar *n*-PrOH ones with $\mu_{n\text{-PrOH}}$ (gas) ~ 1.55 debye (*trans*-conformer) and 1.58 debye (*gauche*-conformer)[39] as well as with the dielectric constant of the liquid state: ε_r (293 K) = 22.2.[40]

According to the standard valence bond theory, the nitroxide radicals can exist in the two limiting resonance structures as neutral or ionic form:[36]

$$>N\text{–}O^{\bullet} \Leftrightarrow >N^{+\bullet}\text{–}O^{-}$$

neutral form ⇔ ionic form

The greater the polarity of a solvent (medium) the more ionic form is favored over the neutral one increasing the electron (charge) density of the oxygen atom, but increasing the spin density on the nitrogen atom.[11,36–38]

On increase the temperature, the $2A_{zz'}$ value in the lowest temperature region begins to decrease above the first characteristic ESR temperature $T_{X1}^{slow,A_{zz}}$(bulk) ~ 130 K due to the partial motional averaging of the magnetic anisotropy of the TEMPO caused by some molecular motion. On further increase the temperature, the most pronounced change of the ESR

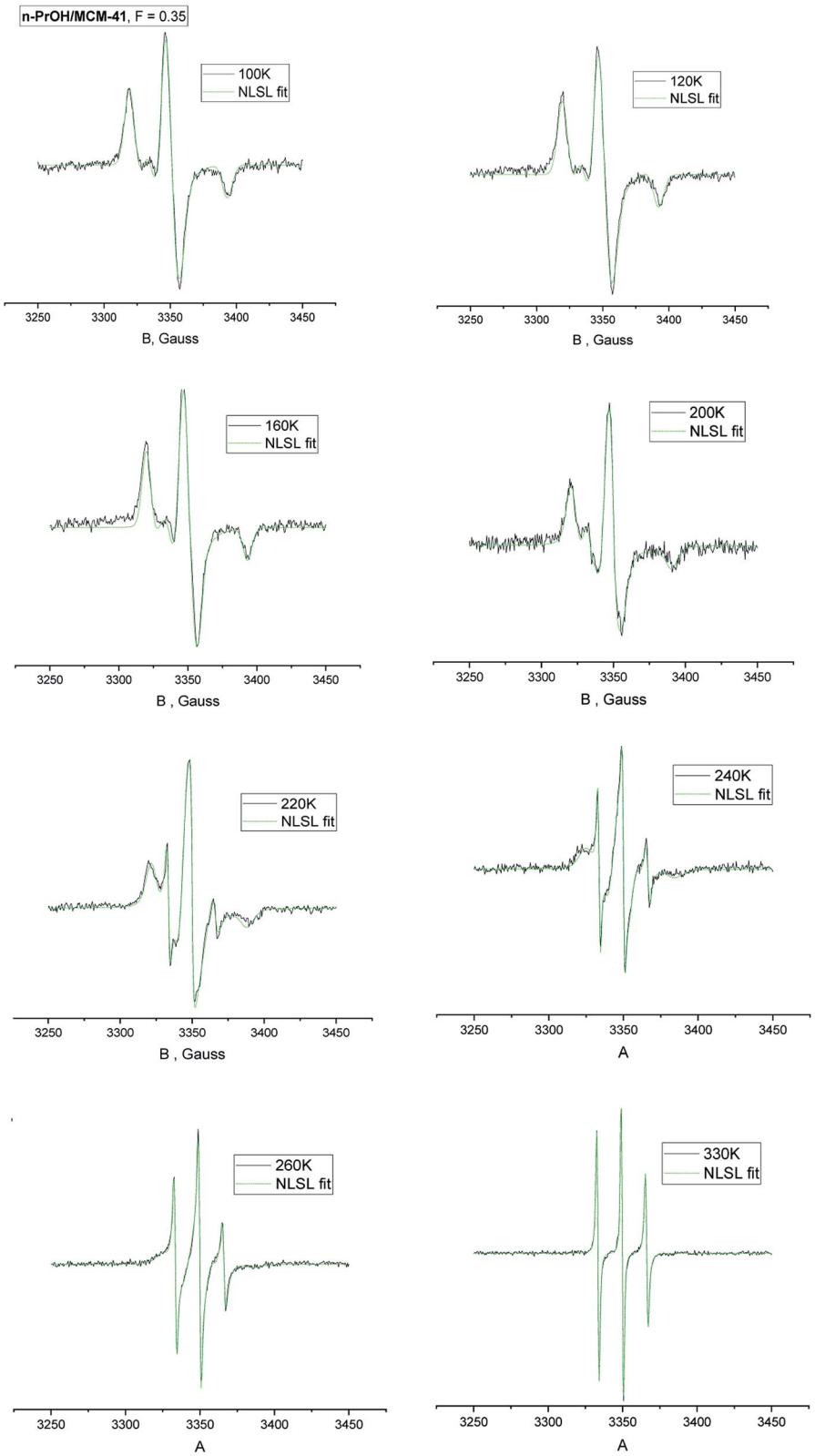

Fig. 1 Typical spectral evolution of the triplet from the spin probe TEMPO in *n*-PrOH confined in MCM-41 matrix at a series of temperatures. Black lines represent the experimental data, the green ones the simulated results.

spectra from the broad to narrow triplet at the conventional characteristic ESR temperature $T_{50\ \mathrm{G}} = 162.5$ K occurs due to a transition from the slow to fast motion regime. After its crossing, two slight changes at $T_{\mathrm{X1}}^{\mathrm{fast},A_{zz}} = 180$ K and $T_{\mathrm{X2}}^{\mathrm{fast},A_{zz}} = 203$ K within the fast motion region take place. The physical origins of all these characteristic ESR temperatures

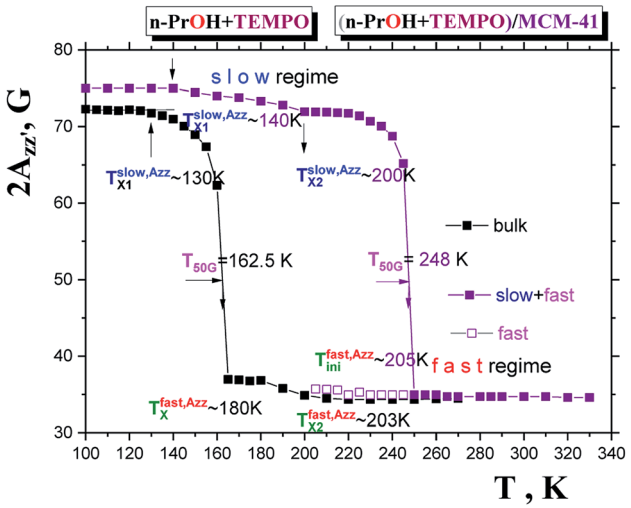

Fig. 2 Spectral parameter $2A_{zz'}$ as a function of temperature for the bulk *n*-PrOH (black points) and for the confined *n*-PrOH/MCM-41 system (violet points). The characteristic ESR temperatures $T_{Xi}^{slow,A_{zz}}$, $T_{50\ G}$ and $T_{Xini}^{fast,A_{zz}}$ as well as $T_{Xi}^{fast,A_{zz}}$ are marked. Error bars are smaller as the point size.

were already partially clarified in ref. 24 and they will be further discussed in the third subsection after presentation of the *o*-Ps data in the next one.

After confinement of *n*-PrOH in the regular virgin MCM-41 matrix the $2A_{zz'}$ *vs.* *T* plot significantly differs in two aspects from that for the bulk *n*-PrOH indicating the large sensitivity of the spin probe ESR technique to the spatial restriction of the confined medium in this special type of silica-based matrix. The first concerns the enhancement of $2A_{zz'}$ (100 K) for TEMPO in the immobilized state at the lowest temperature of our ESR measurements from 72.5 to 75 Gauss. This rather moderate increase for TEMPO in *n*-PrOH embedded in the regular virgin MCM-41 matrix is comparable to that observed in the *n*-PrOH/SG60Å-SIL system with the smallest irregular pores of the virgin SG matrix.[23] It suggests the relative insensitivity to the pore morphology for the roughly similar mean pore size. Note that in the latter case this increase for the larger $D_{pore} = 300$ Å and 100 Å is a bit smaller than for the 60 Å pores suggesting a weak dependence on the extent of spatial limitation of the *n*-PrOH medium.

On the other hand, the increase in $2A_{zz'}$ (100 K) of about 2.5 Gauss for polar *n*-PrOH medium in the confined state with respect to the bulk one is essentially smaller than that for some linear *n*-alkanes (*n*-UND, *n*-HXD) and cycloalkane (CHX) in silicagels investigated so far.[22,29,30] Thus, for the even-number *n*-alkane, *i.e.*, *n*-HXD, the $2A_{zz'}$ (100 K) value changes dramatically from 68 Gauss up to 80 Gauss and $2A_{zz'}$ (300 K) from 33 to up to *ca.* 40 Gauss.[22] For the odd-number *n*-alkane, namely, *n*-UND this increase reaches in $2A_{zz'}$ (100 K) also *ca.* 12 Gauss.[29] Finally, the similar trends were also found for CHX.[30] As evidenced elsewhere,[22,29,30] this significant increase is caused by the bonding interaction of the polar spin probe TEMPO from the very dilute solution in the apolar alkanes and cycloalkane with the polar silanol groups of the virgin SG matrices. As in our regular MCM-41 matrix the pore surface is formed by the same polar silanol groups[41] and the smaller polar molecules of confined *n*-PrOH medium with $D_{n\text{-PrOH}}^{W,eq} = 2.6$ Å are in the overwhelming excess over the larger and very diluted TEMPO ones with $D_{TEMPO}^{W,eq} = 6.8$ Å, these medium's molecules interact preferentially with the surface ≡SiOH groups *via* the interparticle H-bonds. This preferential interaction of the medium's molecules implies in the first approximation the presence of roughly two different kinds of the *n*-PrOH molecules with one part of the molecules in the close vicinity of the surface of the pores formed by the bonded molecules in the "interfacial" region. In addition, because of the amphiphilic character of the *n*-PrOH molecules in the close vicinity to the interface a quasi-ordered phase in the so-called "interphase" region might be formed. The other sort of medium's ones is more distant from the pore surface and thus in the central "core" part of the pore of the MCM-41 matrix. Interestingly, such a structural ordering of the *n*-PrOH molecules was recently evidenced at the surface of the microporous graphite-oxide matrix.[42] This possible structuring of the *n*-PrOH medium's molecules confined in the MCM-41 matrix will be discussed in detail later. Thus, on the basis of the observed moderate increase in $2A_{zz'}$ (100 K) for *n*-PrOH in contrast to the very strong one in various apolar media we can conclude that the "reporter" TEMPO probes reflect dominantly the spatial restriction effect of the MCM-41 matrix on the structural-dynamic state of the polar confined *n*-PrOH.

Another difference between the bulk *n*-PrOH and the confined *n*-PrOH/MCM-41 systems concerns the characteristic ESR temperatures. Fig. 2 shows that within the slow motion regime the two step-wise reductions in $2A_{zz'}$ at occurs at $T_{X1}^{slow,A_{zz}} \sim 140$ K and $T_{X2}^{slow,A_{zz}} \sim 200$ K. The first value is slightly higher compared to the bulk *n*-PrOH. On the other hand, the second one can be apparently related to the bimodal ESR spectrum with the fast spectral component appears at $T_{ini}^{fast,A_{zz}} \sim 205$ K which suggests the dynamic heterogeneity of the used TEMPO molecules in the spatial restricted *n*-PrOH medium *via* the co-existing slow and fast moving spin probes. This aspect will be further discussed in the context with simulations in the next paragraph in detail. The most pronounced slow to fast motion regime transition occurs at the essentially higher $T_{50\ G} = 248$ K, *i.e.*, about 90 K above $T_{50\ G}$ for the bulk *n*-PrOH. It is of interest that the $T_{50\ G}$ (confined) values for *n*-PrOH medium embeded in the irregular virgin SG matrices is significantly smaller reaching of 163, 188 and 193 K for 300 Å, 100 Å and 60 Å pores.[23] This demonstrates the very strong effect of the pore morphology and the pore size distribution being wider for SG's than in the uniform MCM-41 matrix as well as to the pore connectivity with the mutually interconnected pores for SG's *vs.* the isolated ones in MCM-41 matrix on the dynamics of the molecular probe in the investigated confined *n*-PrOH medium.

Fig. 3a and b summarizes the temperature dependences of the correlation times, τ_c^{slow}, τ_c^{fast} and the relative fractions of the slow or/and fast moving spin probes TEMPO, F_{slow}, F_{fast} for both the bulk *n*-PrOH from ref. 24 and the confined *n*-PrOH/MCM-41 systems from spectral simulations as displayed in Fig. 1. Similarities *vs.* differences in both the quantities can be observed. Similarity in the former one, *i.e.*, τ_c consists in the presence of

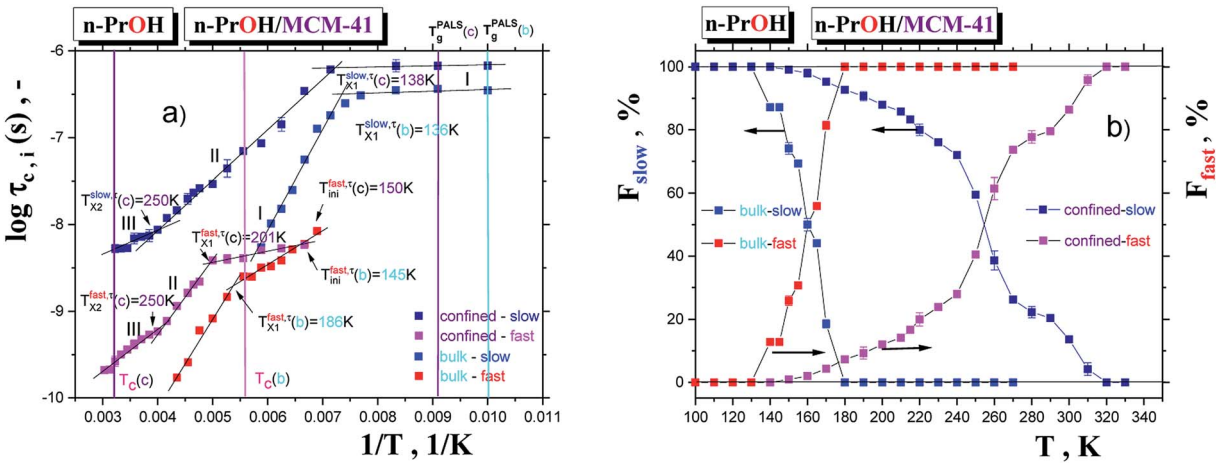

Fig. 3 Correlation times, τ_c^{slow}, τ_c^{fast} (a) and relative fractions F^{slow}, F^{fast} (b) as a function of inverse temperature or temperature, respectively, for the bulk *n*-PrOH (blue and red points) and for the confined *n*-PrOH/MCM-41 system (royal and magenta points). The characteristic ESR temperatures $T_{Xi}^{slow,\tau}$, T_c and $T_{ini}^{fast,\tau}$ and $T_{Xi}^{fast,\tau}$ are marked.

three regions of distinct dynamic behavior. Unimodal spectra at relatively low temperatures from the slow moving TEMPO molecules are followed at intermediate temperatures by the bimodal spectral region of superposed broad and narrow spectra from the co-existing slow and fast reorienting spin probes. Finally, at highest temperatures, the only narrow component from the fast moving TEMPO probes is found. The latter quantity, *i.e.*, *F* closely coupled to the former one exhibit the dominance of the individual spectral components in low- and high-*T* regions and their co-existence in the intermediate temperature ranges.

On the other hand, dramatic differences in the temperature dependencies of the correlation times and the relative fractions are found which reflect the very significant influence of confinement on the dynamics of the probing molecule. Thus, the correlation times in all of the three distinct regions for the confined *n*-PrOH/MCM-41 system are systematically higher indicating large slowing down of the spin probe TEMPO reorientation by the spatial restriction. On crossing the first characteristic ESR temperature $T_{X1}^{slow,\tau} = 136$ K and 138 K in the bulk or confined state, respectively, the onset of the superposed bimodal regions in both the *n*-PrOH systems starts relatively close to the initial ESR temperatures: $T_{ini}^{fast,\tau} = 145$ K and $T_{ini}^{fast,\tau} = 150$ K. Note that the latter value from spectral simulations is essentially lower than that as seen from the extrema line analysis giving $T_{ini}^{fast,A_{zz}} = 203$ K being close rather to the first step temperature $T_{X1}^{slow,A_{zz}} = 140$ K in Fig. 2. Next, at higher temperatures the time scales exhibit diametrically different behaviors. In particular, while in the bulk state the slow component relatively rapidly approaches the fast one over a narrow *T* range at T_c (bulk) ~ 180 K (ref. 24) for the confined one we observed significantly slower reduction with a great separation of the respective correlation times over essentially wider *T* range up to T_c (confined) ~ 310 K. This is accompanied by the difference in the relative fractions being very sharply changing between the two limiting cases over *ca.* 40 K for the bulk *n*-PrOH medium, but very broad for the confined *n*-PrOH/MCM-41 system. Here, the alteration occurs over 170 K with the essential acceleration above *ca.* 240 K towards the purely fast motion regime. Further, in the fast motion regime, three regions are evident with the characteristic ESR temperatures $T_{X1}^{fast,\tau} = 207$ K and $T_{X2}^{fast,\tau} = 250$ K, the last value coincides with that within the slow regime $T_{X2}^{slow,\tau} = 250$ K (Table 2).

These findings of the dynamic heterogeneity of the TEMPO probes in both the bulk and confined *n*-PrOH systems can be interpreted differently but consistently as follows. As shown in ref. 24 dealing with the bulk *n*-PrOH, on the basis of plausible description of the structural dynamics of *n*-PrOH in terms of the two-order parameter (TOP) model and the closely related the spin probe TEMPO reorientation, the co-existence of differently moving spin probes can be ascribed to the presence of the so-called solid-like and liquid-like domains in the bulk *n*-PrOH – Fig. 4. On the other hand, the significantly distinct, *i.e.*, the very slowly decreasing time scale of the slow component in the confined *n*-PrOH/MCM-41 system indicates the localization of a part of the spin probes in some more dense solid-like phase which is qualitatively distinct from that in the bulk medium. This can be associated dominantly with the interphase region being localized in between the interface region, *i.e.* monomolecular layer with the directly interacting *n*-PrOH molecules, but no with the TEMPO ones, and the central "core" part of the pore of the MCM-41 matrix with the more distant *n*-PrOH

Table 2 Activation parameters for the spin probe TEMPO in the confined n-PrOH/MCM-41 system

Regime/region	ΔT K	log τ_∞ (—)	E kJ mol^{-1}	r (—)
Slow-I	100–120	−6.19 ± 0.01	1.98 ± 0.07	0.999
Slow-II	140–250	−10.31 ± 0.08	586.82 ± 15.18	0.996
Slow-III	260–310	−9.15 ± 0.18	267.89 ± 51.3	0.984
Fast-I	150–200	−9.02 ± 0.08	118,13 ± 14.45	0.972
Fast-II	210–250	−12.37 ± 0.15	785.72 ± 34.87	0.996
Fast-III	260–330	−11.31 ± 0.11	537.14 ± 30.88	0.990

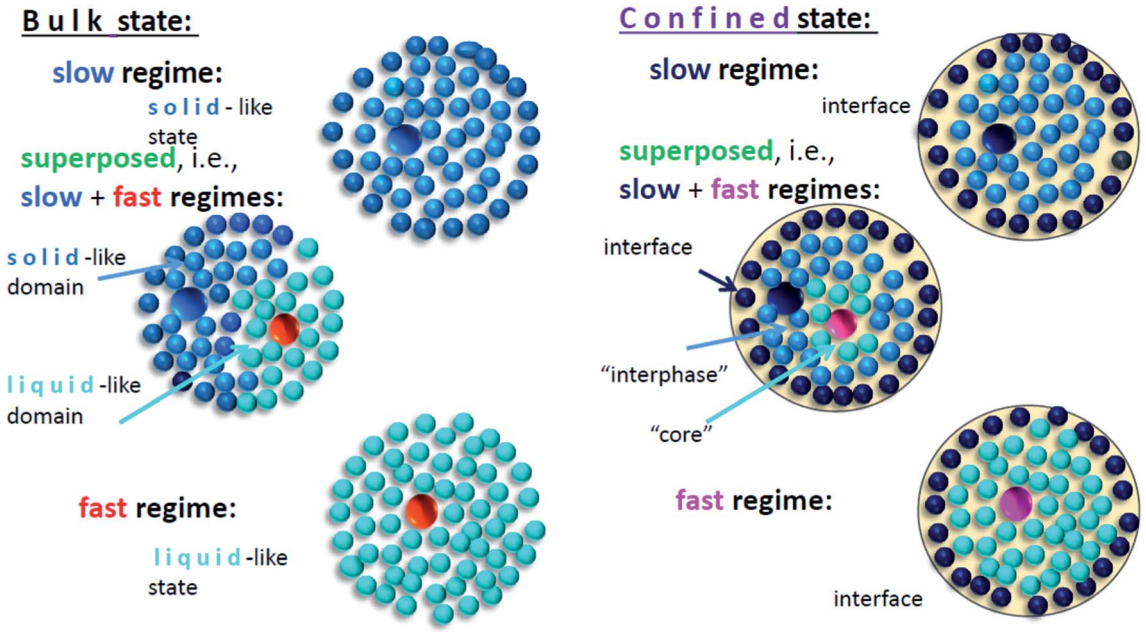

Fig. 4 Schematic model for spin probe TEMPO in the confined *n*-PrOH/MCM-41 system: the slow motion regime in relative low-*T* region and the fast motion regime in relatively high-*T* one as well as the superposed slow – and fast motion regime at intermediate temperatures are depicted. Small and large spheres represent the medium or spin probe molecules, respectively. Variously blue colors for the media molecules and red and violet color for the spin probe ones mark distinct dynamic state of these particles of the bulk and confined systems.

molecules from the pore surface with the quasi-bulk-like behavior influenced by the geometric restriction – see schematic model of polar probe in protic polar medium inserted in polar matrix in Fig. 4.

Note that this schematic model of polar medium imbedded into polar matrix is also consistent with and supported by our recent finding of two relaxation peaks stemming from two distinct dynamic phases in the same *n*-PrOH/MCM-41 saturated system by BDS.[43]

All these findings on the regular MCM-41 matrix together with the previous ones obtained on the irregular SG matrices[23] indicate the different slowing down of spin probe TEMPO mobility as a function of the pore size, the pore size distribution as well as of the pore regularity in the virgin silica-based matrices. This demonstrates the extraordinary ability of the rotation dynamics of small spin probe molecule to reflect sensitively the significant structural-dynamic change in the confined *n*-PrOH medium. The structural-dynamic alteration of *n*-PrOH medium on going from the bulk to the confined state of *n*-PrOH in MCM-41 matrix will be addressed separately in the second sub-section presenting the PALS data and then, the mutual comparison of the molecular mobility data with the free volume behavior will be discussed.

3.2 Free volume holes in the bulk *n*-PrOH and after its confinement in the MCM-41 matrix

Fig. 5 displays the temperature dependence of the *o*-Ps lifetime, τ_3, and of the *o*-Ps lifetime dispersion, σ_3, for both the *n*-PrOH medium in the bulk state[24] and in the confined one after its embedding into the pores of the regular virgin MCM-41 matrix.

In the paper of Gorgol *et al.*[44] a precise study of the porosity of the MCM-41 matrix with surface modifications was performed. The presence of the six components in the annihilation lifetime spectra is realistic in such case, especially for unfilled (empty) or partially filled pores with oligomeric particles. In our work we had completely filled pores of MCM-41 matrix with small molecular entities. As a result, one dominant and other weak, long lived one with about 2% relative intensity *o*-Ps components were observed. Spectral analysis with more components did not yield positive results. The first *o*-Ps component, τ_3, is connected with confined *n*-PrOH medium and the second one, τ_4, with intergrain space. However, the spectral analysis without using the dispersion of short *o*-Ps lifetime gave worse fit variance. A relatively high dispersion value may indicate the presence of other *o*-Ps component with close lifetime values, *e.g.*, the presence of different lifetimes at the boundary of *n*-PrOH and MCM-41. The analysis with the fixation of the *p*-Ps : *o*-Ps intensities to the ratio = 1 : 3 and *o*-Ps dispersion of short *o*-Ps component gave a satisfactory results for our fully filled system.

Both the PALS responses exhibit the course typical for amorphous glass-forming liquids.[18] Four regions of distinct thermal behavior of the *o*-Ps lifetime marked as regions 1–4 can be distinguished with the following three characteristic PALS temperatures: T_g^{PALS}, T_{b1}^{L} and finally, T_{b2}^{L}. In low-*T* range region 1, the absolute mean *o*-Ps lifetime τ_3 is larger and *o*-Ps lifetime dispersion σ_3 essentially larger in the confined *n*-PrOH compared to the bulk *n*-PrOH. This indicates that after confinement of *n*-PrOH in MCM-41 the mean free volume hole is increased and free volume dispersion is strongly

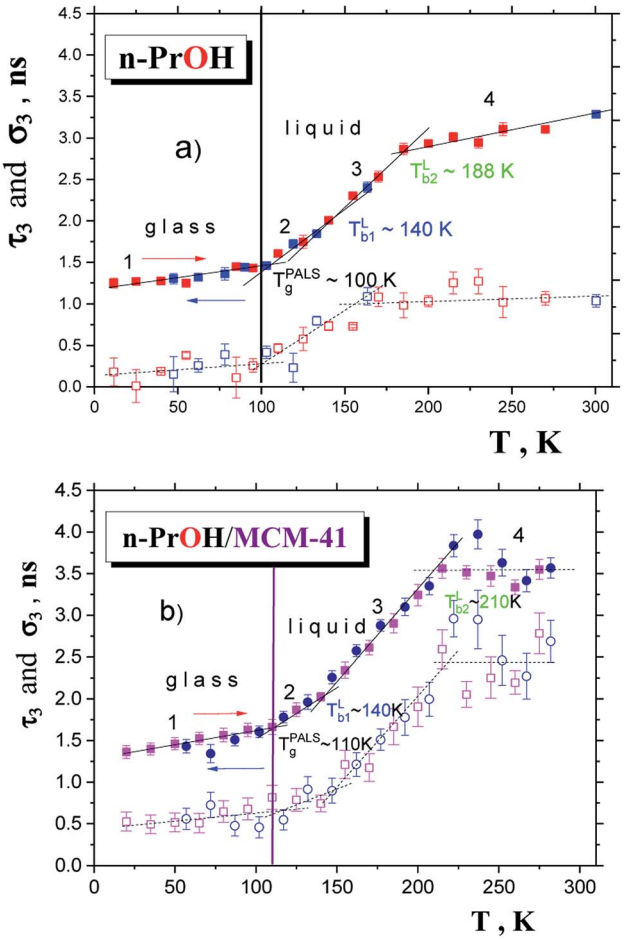

Fig. 5 *o*-Ps lifetime, τ_3, (full points) and *o*-Ps lifetime dispersion, σ_3, (empty points) as a function of temperature for the bulk *n*-PrOH (a) with red and blue points for heating or cooling runs, respectively, and for the confined *n*-PrOH/MCM-41 system (b) with pink and royal points for heating or cooling runs, respectively. The characteristic PALS temperatures T_g^{PALS}, T_{b1}^{L} and T_{b2}^{L} are depicted.

redistributed in such a way that it is larger than those in the bulk state. Similar although more pronounced effect for τ_3 was found also for polyalcohol, namely, 1,2,3-propantriol (glycerol) in ref. 17. On increase the temperature, the first pronounced bend effects at the first characteristic PALS temperatures, being typical for the glass-to-liquid transition, occur at T_g^{PALS} (bulk) = 100 K (ref. 24) and T_g^{PALS} (confined) ≅ 110 K. Similar moderate increase in the T_g^{DSC} values was observed for other amorphous hydrogen-bonded glass-formers, such as polyols: 1,2-propanediol (propylene glycol) and 1,2,3-propanetriol (glycerol) embedded in irregular (CPG, Vycor) and regular (MCM-41) silica-based matrices by classic DSC technique.[45] In the next region 2, the mean τ_3 and σ_3 values for the confined *n*-PrOH/MCM-41 system are still slightly higher indicating a continuing increase of the mean free volume hole size as well as its dispersion in the liquid state due to geometrical restriction. On further increase the temperature, a weak change in the slope of τ_3 *vs.* *T* at T_{b1}^{L} (confined) = 146 K is slightly shifted with respect to T_{b1}^{L} (bulk) = 139 K. On the other hand, a pronounced difference in the corresponding σ_3 *vs.* *T* dependences is found indicating a large broadening of the free volume distribution in the geometrically restricted *n*-PrOH. While in the bulk *n*-PrOH it becomes low and constant up to the final temperature of our measurement at 300 K, in the confined state it continues relative sharply up to *ca.* 212 K only. Finally, region 3 is followed by region 4 with the second dramatic change of slope as well as of type of temperature dependence. Thus, while in the bulk state an increasing trend is similar to that for longer *n*-alkanols starting from *n*-hexanol,[46] in the confined *n*-PrOH/MCM-41 system it becomes approximately quasi-constant with the higher τ_3 value. The characteristic PALS temperature T_{b2}^{L} (bulk) = 180 K in the bulk *n*-PrOH is increased in the confined state toward T_{b2}^{L} (confined) ≈ 212 K. As already mentioned, the dispersion parameter in the bulk *n*-PrOH remains constant above T_{b1}^{L} up to RT, while in the confined state it becomes roughly constant above T_{b2}^{L} (confined) up to RT.

3.3 On the mutual relationships between molecular mobility of TEMPO and free volume hole behavior in *n*-PrOH in the bulk and the confined state in MCM-41 matrix

Fig. 6 and 7 compare of the spin probe TEMPO mobility in terms of $2A_{zz'}$ and τ_c, respectively, with the *o*-Ps annihilation ones obtained from the PALS data using LT polymers programme[34] from a combination of the corresponding ESR and PALS responses in the bulk and confined states from Fig. 2 and 3 or 5, respectively.

3.3.1 Bulk *n*-PrOH + TEMPO system. In our previous joint ESR and PALS as well as broadband dielectric spectroscopy (BDS). Study on the bulk *n*-PrOH[24] it was already demonstrated that the observed changes in the spin probe TEMPO mobility in the liquid state correlate with alternations in the mean *o*-Ps lifetime as extracted from PALS spectra using PATFIT programme[47] and the related mean free volume expansions and that these can be related to the structural relaxation time scale from BDS. In the present work, the same PALS data on *n*-PrOH were evaluated using advanced LT programme[34] giving not only the mean *o*-Ps lifetime τ_3, but also its dispersion, σ_3 which provide richer and more detailed information about the free volume microstructure in terms of not only mean free volume, but also its distribution. Note that the mean *o*-Ps lifetimes as obtained from LT routine are very close to those from PATFIT one with the almost same characteristic PALS temperatures. Thus, as seen in Fig. 6a, the first motional averaging of the magnetic anisotropy of TEMPO at $T_{X1}^{slow,A_{zz}}$(bulk) ~ 130 K lies in the vicinity of the first change in slope of *o*-Ps lifetime at T_{b1}^{L} (bulk) = 139 K from Fig. 5a coinciding with the change in free volume expansion due to the change in the dynamic state from the strongly to weakly supercooled liquid *n*-PrOH. This $T_{X1}^{slow,A_{zz}}$(bulk) ≡ T_{b1}^{L}(bulk) relationship can be related to the dynamic crossover temperature $T_X^{PL} = T_c^{MCT}$ = 139 K from the power law for viscosity as a function of temperature[48,49] and its theoretical rationalization in terms of the idealized mode coupling theory (I-MCT).[50] Alternative explanation for this as well as for further characteristic ESR temperatures within the fast motion regime is mentioned below.

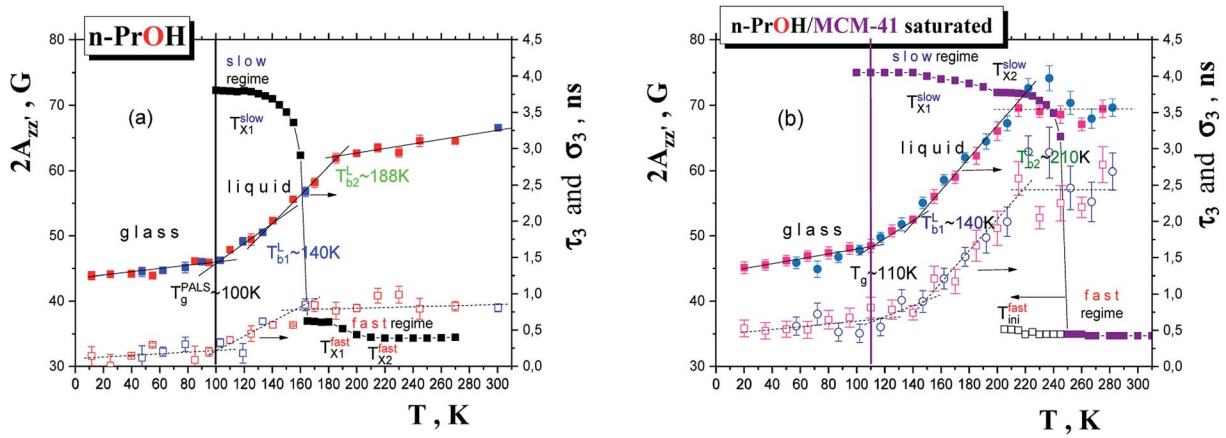

Fig. 6 Comparison between the spectral parameter, $2A_{zz'}$, and the *o*-Ps lifetime, τ_3, and *o*-Ps dispersion, as a function of temperature for the bulk *n*-PrOH (a) and for the confined *n*-PrOH/MCM-41 (b). In the former case coincidences between the characteristic ESR and PALS temperatures $T_{X1}^{slow} \approx T_{b1}^{L}$ and $T_{X1}^{fast} \approx T_{b2}^{L}$, while in the latter one coincidences between the characteristic ESR and PALS temperatures $T_{X1}^{slow,A_{zz}} \cong T_{b1}^{L}$ and $T_{X1}^{slow,A_{zz}} \cong T_{Xini}^{fast,A_{zz}} \cong T_{b2}^{L}$ are evident.

The slow to fast motion regime transition as operationally characterized by $T_{50\ G}$, corresponding the time scale of re-orientation reaches a few ns[11,24,51] has no direct counterpart in the PALS data because of the conventional nature of the operational definition as mentioned already in ref. 24. The next first change in the spin probe TEMPO dynamics within the fast regime at $T_{X1}^{fast,A_{zz}}(\text{bulk}) = 180$ K coincides with the strongly reduced slope above $T_{b2}^{L}(\text{bulk}) = 180$ K in the τ_3 *vs.* *T* plot. This latter effect is the well known fact of the PALS technique connected with the specific interaction between the quantum-mechanical *o*-Ps particle and the very low viscosity medium giving to rise the so-called bubble-like type of free volume.[44] Further, both these high-*T* ESR and PALS phenomena well correlate with the higher-*T* dynamic crossover from the non-Arrhenius to Arrhenius regime of the structural relaxation dynamics of *n*-PrOH at $T_A = 179$ K.[24] Then, it was concluded that in contrast to the saturation effect in *o*-Ps annihilation the change in molecular probe dynamics is the real physical phenomenon which reflects directly a subtle change in the structural-dynamic state of the bulk *n*-PrOH medium.[24] Finally, most of these coinciding relationships between the corresponding characteristic ESR and PALS temperatures can be

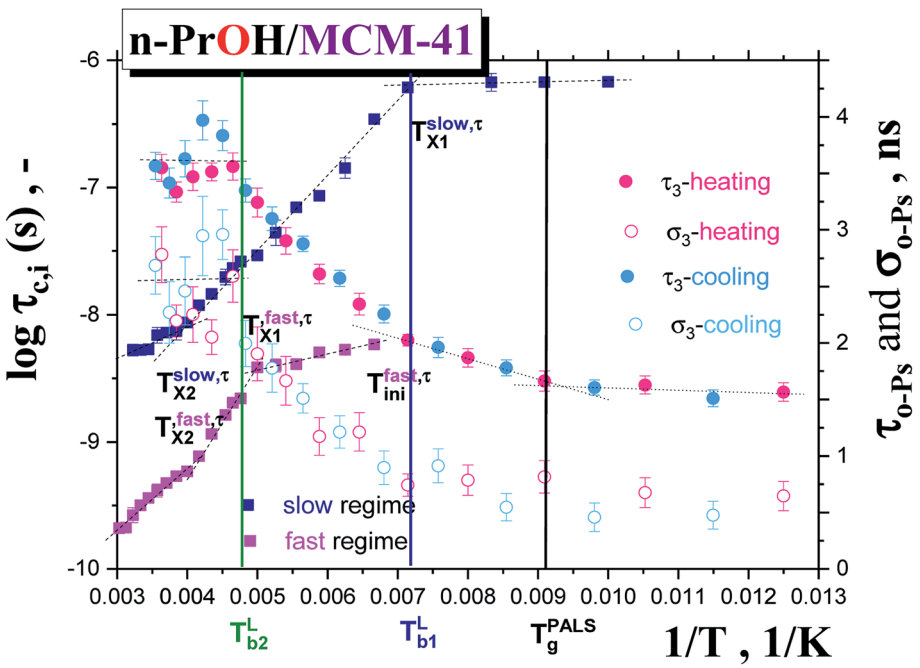

Fig. 7 Arrhenius plot for log of correlation times $\tau_{c,i}$ against $1/T$ *vs.* *o*-Ps lifetime τ_3 and *o*-Ps lifetime dispersion, σ_3 against $1/T$ for the confined *n*-PrOH/MCM-41 system. The characteristic ESR and PALS temperatures are depicted showing close coincidences – see more in the text.

interpreted in terms of the two-order parameter (TOP) model *via* the mutually related evolution with temperature of the liquid-like domains and the solid-like ones in the supercooled liquid and normal liquid state of bulk *n*-PrOH.[24]

3.3.2 Confined (*n*-PrOH + TEMPO)/MCM-41 saturated system. Fig. 6b presents the mutual comparison of ESR response from Fig. 2 with PALS one from Fig. 5b for the confined *n*-PrOH/MCM-41 system. In sharp contrast to the bulk *n*-PrOH, essentially wider range of the slow motion regime is observed with the slightly shifted and some new characteristic ESR temperatures with respect to the bulk state given in Fig. 6a. Thus, the first change in $2A_{zz'}$ *vs.* T plot occuring at $T_{X1}^{slow,A_{zz}}$(confined) $\sim$ 140 K is close to the change in slope at T_{b1}^{L} (confined) $\sim$ 146 K in τ_3 *vs.* T dependence. This coincidence suggests that the molecular motion causing the first free volume expansion in the liquid state of the confined *n*-PrOH is responsible also for the change in the spin probe mobility in this low-T region. Moreover, as mentioned above in ESR section, this change suggests the bulk-like behavior in some local region (s) of the confined *n*-PrOH is (are) present.

On increase the temperature, the high $2A_{zz'}$ values persist up to $T_{X2}^{slow,A_{zz}} \sim 200$ K in consistence with the first visible appearance of the fast component at $T_{ini}^{fast,A_{zz}} \sim 205$ K. This long-T range persisting existence of the slow spectral component roughly coincides with the onset of the quasi-plateau region in the PALS response in both the *o*-Ps annihilation quantities, *i.e.*, not only the mean *o*-Ps lifetime, but also and mainly with the *o*-Ps dispersion above $T_{b2}^{L} \sim 210$ K. As already mentioned in the context with the bulk *n*-PrOH, this saturation effect is the artefact of PALS techniques and this effect is consistent with a qualitative change in the investigated system as seen by molecular probe. It is of interest that the mean bubble size in the confined *n*-PrOH medium is larger in comparison with that in the bulk *n*-PrOH medium, but it seems to be plausible with an essentially broader distribution of the *o*-Ps lifetimes and that of related free volume which could allow for a formation of larger bubbles.

By analogy to the bulk *n*-PrOH, this high-T region above T_{b2}^{L} (confined) $\sim$ 210 K consists in a formation of the so-called bubble-like type of the free volume. Since as it is indicated by the PALS data, the confinement of *n*-PrOH in MCM-41 matrix is associated with the significant rearrangement of the *n*-PrOH constituents within the pores of the MCM-41 matrix reflected by increased mean *o*-Ps lifetime, τ_3, and related mean free volume as well as with the very wide dispersion of *o*-Ps lifetime σ_3 and related free volume dispersion within the regular pores of the MCM-41 matrix with respect to the bulk situation, our observation of the higher τ_3 value above T_{b2}^{L} suggests again the highly heterogeneous character of the confined medium with some local regions of lower viscosity allowing for a creation of the larger bubble-like states of *o*-Ps with respect to the bulk *n*-PrOH. On the other hand, two further changes in the characteristic ESR temperature within the slow regime at T_{X2}^{slow} and the onset of the fast moving TEMPO molecules at T_{ini}^{fast} appear to be consistent with the occurence of the bubble-like form of free volume around T_{b2}^{L} as in the case of the bulk *n*-PrOH.

Finally, the most pronounced effect in the ESR spectra in the $2A_{zz'}$ *vs.* T plot is connected with the pronounced motional averaging of the magnetic anisotropy as represented by the $2A_{zz'}$ *vs.* T dependence and related transition of spin probe TEMPO dynamics from the slow to fast motion regime.[11] This is conventionally defined by the characteristic ESR temperature $T_{50\ G}$ which is connected with the time scale of reorientation of a few nanoseconds.[11,24] Thus, the finding $T_{50\ G}$ (bulk) = 162.5 K *vs.* $T_{50\ G}$ (confined) $\sim$ 248 K.

Another type of ESR *vs.* PALS data comparison for the confined *n*-PrOH/MCM-41 system in terms of the relevant time scales is given in Fig. 7. Similarly as for previously shown $2A_{zz'}$ parameter, two coincidences can be revealed.

In the low-T region, the first change in the slope of slow motion regime at around $T_{X1}^{slow,\tau}$ (confined) = 150 K close to the onset of the fast motion component as obtained from the detailed NLSL simulations at $T_{ini}^{fast,\tau} \cong 145$ K is coinciding with the first characteristic PALS temperature of the free volume expansion in the liquid phase at $T_{b1}^{L} = 140$ K. Note that the onset of the fast component as seen from the spectral simulations appears at the essentially lower temperature compared to the estimated $T_{ini}^{fast,A_{zz}} \sim 205$ K as obtained from simple visual inspection and evaluation of the ESR spectra *via* WINEPR programme. Similar finding was revealed also for the bulk *n*-PrOH[24] as well as for one amorphous polymer, *cis*-1,4-poly(isoprene) (*cis*-1,4-PIP).[51]

On increase the temperature, the first change in the fast dynamics of the TEMPO molecules occurs just at $T_{X1}^{fast,\tau} \sim 207$ K in the vicinity of the strongly shifted onset of the quasi-saturated region above $T_{b2}^{L} = 210$ K. This coincidence suggests the localization of a part of the fast moving probes in the bulk-like regions of the *n*-PrOH/MCM-41 system and thus, their sensitivity to the elevated temperature of the confined system. Simultaneously, on the other hand, the slow component persists with continuously slowly decreasing time scale, τ_c^{slow} and decreasing population fraction F^{slow} up to $T_c = 310$ K. These specific trends are very strongly distinct from the bulk *n*-PrOH[24] and suggest on the localization of the slow moving probes in some more dense zone of the confined system. We ascribe this more dense zone to the interphase region in between the interface region with the *n*-PrOH molecules bound to the silanol surface groups of the MCM-41 matrix and the inner "core" region with the bulk-like behavior of the *n*-PrOH molecules. All these findings appear to be qualitatively consistent with the proposed schematic model of polar probe dissolved in polar medium confined in polar matrix in Fig. 4.

4. Conclusions

The characterizations of the confinement effect on typical protic polar organic medium, *n*-propanol inserted in the regular virgin silica MCM-41 matrix by means of two microscopic *i.e.*, molecular-sized TEMPO and atomic-sized *o*-Ps probe particles using ESR or PALS, respectively, are reported. Significant alterations in the spectral features of TEMPO in the confined state with respect to those in the bulk *n*-PrOH medium reflect essential changes in the dynamic behavior of the used spin

probe in both spin systems. At the same time, very significant alteration in the *o*-Ps annihilation, especially in the *o*-Ps lifetime dispersion, compared to the bulk *n*-PrOH medium indicates a drastic redistribution of the free volume holes after spatial limitation resulting especially in broadening of the free volume hole distribution. By mutual comparison of the ESR and PALS responses, numerous coincidences between the characteristic ESR and PALS temperatures are revealed which suggest the common physical origin of the respective changes in these microscopic responses as seen by molecular and atomic-sized probes. This joint study emphasizes the appropriate choice of the filler-confiner pair in the confined organic medium to get the reliable microscopic information about its altered structural-dynamic state with respect to its reference bulk situation.

Conflicts of interest

We declare no conflict of interests.

Acknowledgements

This work was supported by the Slovak Research and Development Agency (SRDA) under the contract no. APVV-16-0369. We also thank the VEGA Agency, Slovakia for grant no. 2/0030/16.

References

1 P. Huber, *J. Phys.: Condens. Matter*, 2015, **27**, 103102.
2 (*a*) M. Koza, B. Frick and R. Zorn, *Eur. Phys. J. Spec. Top.*, 2010, **189**, special issue; (*b*) M. Koza, B. Frick and R. Zorn, *Eur. Phys. J. Spec. Top.*, 2007, **141**, special issue; (*c*) M. Koza, B. Frick and R. Zorn, *Eur. Phys. J. E*, 2003, **12**, special issue; (*d*) B. Frick, R. Zorn and H. Büttner, *J. Phys. IV*, 2000, **10**, special issue.
3 C. Alba-Simionesco, B. Coasne, G. Dosseh, G. Dudziak, K. E. Gubbins, R. Radhakrishnan and M. Sliwinska-Bartkowiak, *J. Phys.: Condens. Matter*, 2006, **18**, R15.
4 M. Alcoutlabi and G. B. McKenna, *J. Phys.: Condens. Matter*, 2005, **17**, R46.
5 (*a*) *Dynamics in Geometrical Confinement*, ed. F. Kremer, Springer, Heidelbeg, 2014; (*b*) R. Richert, *Annu. Rev. Phys. Chem.*, 2011, **62**, 65.
6 (*a*) A. A. Schönhals, R. Zorn and B. Frick, *Polymer*, 2016, **105**, 393; (*b*) M. Kruteva, A. Wischnevski and D. Richter, *Phys. J. Conf.*, 2015, **83**, 2009–2011.
7 J. M. Drake and J. Klafter, *Phys. Today*, 1990, **43**, 46.
8 W. D. Dozier, J. M. Drake and J. Klafter, *Phys. Rev. Lett.*, 1986, **56**, 197.
9 M. K. Mundra, C. J. Ellison, P. Rittigstein and J. M. Torkelson, *Eur. Phys. J. Spec. Top.*, 2007, **141**, 143.
10 (*a*) G. Dlubek, in *Encyclopedia of Polymer Science and Technology*, ed. A. Siedel, Wiley & Sons, Hoboken, 2008; (*b*) *Principles and Application of Positron and Positronium Chemistry*, ed. Y. C. Jean, P.E. Malton and D. S. Schrader, World Scientific, Singapore, 2003.
11 (*a*) R. Owenius, M. Engstrom, M. Lindgrem and M. Huber, *J. Phys. Chem. A*, 2001, **105**, 10967; (*b*) R. Improta and V. Barone, *Chem. Rev.*, 2004, **104**, 1231; (*c*) G. G. Cameron, in *Comprehensive Polymer Science*, ed. C. Booth and C. Price, vol. 1, Pergamon Press, Oxford, 1989, pp. 517–541; (*d*) *Spin Labelling Theory and Applications*, ed. L. J. Berliner, Academic Press, New York, 1976.
12 T. Kamijo, A. Yamaguchi, S. Suzuki, N. Teramae, T. Itoh and T. Ikeda, *J. Phys. Chem. A*, 2008, **112**, 11535.
13 M. Roussenova, M. A. Alam, S. Townrow, D. Kilburn, P. E. Sokol, R. Guillet-Nicolas and F. Kleitz, *New J. Phys.*, 2014, **16**, 103030–103031.
14 R. Zaleski and J. Goworek, *Mater. Sci. Forum*, 2009, **607**, 180.
15 M. Iskrová, V. Majerník, E. Illeková, O. Šauša, D. Berek and J. Krištiak, *Mater. Sci. Forum*, 2009, **607**, 235.
16 D. Dutta, P. K. Pujari, K. Sudarshan and S. K. Sharma, *J. Phys. Chem. C*, 2008, **112**, 19055.
17 D. Kilburn, P. E. Sokol, V. G. Sakai and M. A. Alam, *Appl. Phys. Lett.*, 2008, **92**, 33109–33111.
18 (*a*) J. Bartoš, O. Šauša, P. Bandžuch, J. Zrubcová and J. Krištiak, *J. Non-Cryst. Solids*, 2002, **307–310**, 417; (*b*) G. Dlubek, M. Q. Shaikh, K. Raetzke, M. Paluch and F. Faupel, *J. Phys.: Condens. Matter*, 2010, **22**, 235104; (*c*) W. Salgueiro, A. Somoza, L. Silva, G. Consolati, F. Quasso, M. A. Mansilla and A. Marzocca, *Phys. Rev. E: Stat., Nonlinear, Soft Matter Phys.*, 2011, **83**, 051805.
19 S. Anandan and M. Okazaki, *Microporous Mesoporous Mater.*, 2005, **87**, 77.
20 (*a*) G. Martini, M. F. Ottaviani, M. Romanelli and L. Kevan, *Colloids Surf.*, 1989, **41**, 149; (*b*) G. Martini, *Colloids Surf.*, 1990, **45**, 83.
21 H. Yoshioka, *J. Chem. Soc., Faraday Trans. 1*, 1988, **84**, 4509.
22 M. Lukešová, H. Švajdlenková, P. Sippel, E. Macová, D. Berek, A. Loidl and J. Bartoš, *Eur. Phys. J. B*, 2015, **88**, 46.
23 J. Bartoš, M. Lukešová, H. Švajdlenková and O. Šauša, *AIP Conf. Proc.*, 2018, **1981**, 020081.
24 J. Bartoš, H. Švajdlenková, O. Šauša, M. Lukešová, D. Ehlers, M. Michl, P. Lunkenheimer and A. Loidl, *J. Phys.: Condens. Matter*, 2016, **28**, 015101–1.
25 (*a*) J. Bartoš, H. Švajdlenková, R. Zaleski, M. Edelmann and M. Lukešová, *Physica B*, 2013, **430**, 99; (*b*) M. Lukešová, B. Zgardzinska, H. Švajdlenková, R. Zaleski and B. Charmas, *Phys. B*, 2015, **476**, 100; (*c*) J. Bartoš, B. Zgardzinska, H. Švajdlenková, M. Lukešová and R. Zaleski, *Chem. Phys. Lett.*, 2018, **700**, 102; (*d*) J. Bartoš, H. Švajdlenková, Y. Yu, G. Dlubek and R. Krause-Rehberg, *Chem. Phys. Lett.*, 2013, **584**, 88; (*e*) J. Bartoš, H. Švajdlenková, M. Lukešová, Y. Yu and R. Krause-Rehberg, *Chem. Phys. Lett.*, 2014, **602**, 28; (*f*) J. Bartoš, C. Corsaro, M. Mallamace, H. Švajdlenková and M. Lukešová, *Phys. Chem. Chem. Phys.*, 2018, **20**, 1145.
26 J. Bartoš and H. Švajdlenková, *Chem. Phys. Lett.*, 2017, **670**, 58.
27 H. Švajdlenková, M. Iskrová, O. Šauša, G. Dlubek, J. Krištiak and J. Bartoš, *Macromol. Symp.*, 2011, **305**, 108.

28 H. Švajdlenková, O. Šauša, M. Iskrová-Miklošovičová, V. Majerník, J. Krištiak and J. Bartoš, *Chem. Phys. Lett.*, 2012, **539–540**, 39.
29 J. Bartoš, O. Šauša, H. Švajdlenková, I. Mařko and K. Čechová, *J. Non-Cryst. Solids*, 2019, **511**, 1.
30 M. Lukešová, H. Švajdlenková, D. Reuter, S. Valič, A. Loidl and J. Bartoš, *Chem. Phys. Lett.*, 2019, **735**, 136756.
31 (*a*) Ch. T. Kresge and W. J. Roth, *Chem. Soc. Rev.*, 2013, **42**, 3663; (*b*) J. S. Beck, J. C. Vartuli, W. J. Roth, M. E. Leonowicz, K. D. Schmidt, C. T. W. Chu, D. H. Olson, E. W. Sheppard, S. B. McCullen, J. B. Higgins and J. L. Schlenker, *J. Am. Chem. Soc.*, 1992, **114**, 10834; (*c*) C. T. Kresge, M. E. Leonowicz, W. J. Roth, J. C. Vartuli and J. S. Beck, *Nature*, 1992, **359**, 710.
32 G. P. Rabold, *J. Polym. Sci., Part A-1: Polym. Chem.*, 1969, **17**, 1203.
33 D. E. Budil, S. Lee, S. Saxena and J. H. Freed, *J. Magn. Reson., Ser. A*, 1996, **120**, 155.
34 J. Kansy, *Nucl. Instrum. Methods Phys. Res., Sect. A*, 1996, **374**, 235.
35 (*a*) S. J. Tao, *J. Chem. Phys.*, 1972, **56**, 5499; (*b*) M. Eldrup, D. Lightbody and J. N. Sherwood, *Chem. Phys.*, 1981, **63**, 51; (*c*) H. Nakanishi, Y. C. Jean and S. J. Wang, in *Positron Annihilation Studies of Fluids*, ed. S. C. Sharma, World Scientific, Singapore, 1988, p. 292; (*d*) B. Jasinska, A. E. Koziol and T. Goworek, *J. Radioanal. Nucl. Chem.*, 1996, **210**, 617; (*e*) G. Consolati, *J. Chem. Phys.*, 2002, **117**, 7279.
36 (*a*) H. G. Aurich, K. Hahn and W. Weiss, *Tetrahedron*, 1977, **33**, 969; (*b*) B. R. Knauer and J. J. Napier, *J. Am. Chem. Soc.*, 1976, **98**, 4395; (*c*) O. H. Griffith, P. J. Dehlinger and S. P. Van, *J. Membr. Biol.*, 1974, **15**, 159; (*d*) A. H. Reddoch and S. Konishi, *J. Chem. Phys.*, 1979, **70**, 2121; (*e*) I. Al-Balaa and R. D. Bates Jr, *J. Magn. Reson.*, 1987, **73**, 78; (*f*) T. Abe, S. Tero-Kubota and Y. Ikegami, *J. Phys. Chem.*, 1982, **86**, 1358; (*g*) T. Yagi and O. Kikuchi, *J. Phys. Chem. A*, 1999, **103**, 9132.
37 M. A. Ondar, O. Y. Grinberg, A. A. Dubinskii and Y. S. Lebedev, *Sov. J. Chem. Phys.*, 1985, **3**, 781.
38 J. Lalevee, X. Allonas and P. Jaques, *J. Mol. Struct.: THEOCHEM*, 2006, **767**, 143.
39 *Rosamonte's Physical Chemistry Website*.
40 J. A. Dean, *Handbook of Organic Chemistry*, New York, NY, McGraw-Hill Book Co., 1987, pp. 4–73.
41 (*a*) A. Jentys, K. Kleestorfer and H. Vinek, *Microporous Mesoporous Mater.*, 1999, **27**, 321; (*b*) A. Jentys, N. H. Pham and H. Vinek, *J. Chem. Soc., Faraday Trans.*, 1996, **92**, 3287; (*c*) J. Chen, Q. Li, R. Xu and F. Xiao, *Angew. Chem., Int. Ed. Engl.*, 1995, **34**, 2694.
42 C. Cabrillo, F. Barroso-Bujans, R. Rodrigues-Peresa, F. Fernandes-Alonso, D. Bowron and F. J. Bermejo, *Carbon*, 2016, **100**, 546.
43 (*a*) H. Švajdlenková, S. Arrese-Igor, A. Kleinová, A. Alegria and J. Bartoš, *Abstract at European Soft Matter Infrastructure (EUSMI) Annual Meeting*, Portonovo, Italy, 2019; (*b*) J. Bartoš, H. Švajdlenková, S. Arese- Igor, A. Kleinova and A. Alegria, *Polymers*, submitted.
44 M. Gorgol, P. Krasucka, J. Goworek and R. Zaleski, *Acta Phys. Pol., A*, 2017, **132**, 1559.
45 (*a*) W. Zheng and S. L. Simon, *J. Chem. Phys.*, 2007, **127**, 194501; (*b*) O. Trofymluk, A. A. Levchenko and A. Navrotskya, *J. Chem. Phys.*, 2005, **123**, 194509–194511; (*c*) J. Zhang, G. Liu and J. Jonas, *J. Phys. Chem.*, 1992, **96**, 3478.
46 B. Zgardzinska and T. Goworek, *Chem. Phys.*, 2012, **405**, 32.
47 P. Kirkegaard, M. Eldrup, O. E. Mogensen and N. J. Pedersen, *Comput. Phys. Commun.*, 1989, **23**, 307.
48 P. Taborek, R. N. Kleinman and D. J. Bishop, *Phys. Rev. B: Condens. Matter Mater. Phys.*, 1986, **34**, 1835.
49 F. Mallamace, C. Branca, C. Corsaro, N. Leone, J. Spooren, S. H. Chen and H. E. Stanley, *Proc. Natl. Acad. Sci. U. S. A.*, 2010, **107**, 22457.
50 (*a*) W. Götze, *J. Phys.: Condens. Matter*, 1999, **11**, A1–A45; (*b*) W. Götze and L. Sjogren, *Rep. Prog. Phys.*, 1992, **55**, 241.
51 H. Švajdlenková, S. Arrese-Igor, Z. Nógellová, A. Alegrıía and J. Bartoš, *Phys. Chem. Chem. Phys.*, 2017, **19**, 15215.

